Island Arc

High-resolution upper Pliocene to Pleistocene calcareous nannofossil biostratigraphy in Ocean Drilling Program Hole 1146A in the South China Sea

Journal:	*Island Arc*
Manuscript ID	IAR-20-0074.R2
Manuscript Type:	Research Article
Date Submitted by the Author:	n/a
Complete List of Authors:	Emanuel, Sara; Tohoku University, Department of Earth Science Sato, Tokiyuki; Akita University, Department of Earth Resource Science, Faculty of International Resource Sciences Chiyonobu, Shun; Akita University, Earth Resource Science Shyu, J. Bruce H.; National Taiwan University, Department of Geosciences Bassi, Davide; University of Ferrara, Dipartimento di Fisica e Scienze della Terra Iryu, Yasufumi; Tohoku University, Institute of Geology and Paleontology, Graduate School of Science;
Key words:	Biostratigraphy, Calcareous nannofossil, First occurrence, Last occurrence, Ocean Drilling Program, Pliocene-Pleistocene, South China Sea

High-resolution upper Pliocene to Pleistocene calcareous nannofossil biostratigraphy in Ocean Drilling Program Hole 1146A in the South China Sea

SARA EMANUEL*[1], TOKIYUKI SATO[2], SHUN CHIYONOBU[2], J. BRUCE H. SHYU[3], DAVIDE BASSI[4], YASUFUMI IRYU[1]

[1] *Institute of Geology and Paleontology, Graduate School of Science, Tohoku University, Sendai, Japan*

[2] *Department of Earth Resource Science, Faculty of International Resource Sciences, Akita University, Akita, Japan*

[3] *Department of Geosciences, National Taiwan University, Taipei, Taiwan*

[4] *Dipartimento di Fisica e Scienze della Terra, Università degli Studi di Ferrara, Ferrara, Italy*

*Correspondence

Author email addresses

Sara Emanuel: saraemanuel17@gmail.com

Tokiyuki Sato: toki@gipc.akita-u.ac.jp

Shun Chiyonobu: chiyo@gipc.akita-u.ac.jp

J. Bruce H. Shyu: jbhs@ntu.edu.tw

Davide Bassi: bsd@unife.it

Yasufumi Iryu: yasufumi.iryu.d8@tohoku.ac.jp

Conflicts of interest

The authors have no conflicts of interest to declare.

Availability of data and materials

Please contact the corresponding author regarding data requests.

Abstract

We established a high-resolution calcareous nannofossil biostratigraphy for the late Pliocene–Pleistocene by analyzing a 242 m-thick, continuous sedimentary succession from Ocean Drilling Program Site 1146, Hole A, in the South China Sea (SCS). A total of 14 calcareous nannofossil datums were detected in the SCS succession. They are, in descending order: first occurrence (FO) of *Emiliania huxleyi*, last occurrence (LO) of *Pseudoemiliania lacunosa*, LO of *Reticulofenestra asanoi*, FO of *Gephyrocapsa parallela*, FO of *R. asanoi*, LO of large *Gephyrocapsa* spp., FO of large *G.* spp., FO of *Gephyrocapsa oceanica*, FO of *Gephyrocapsa caribbeanica*, LO of *Calcidiscus macintyrei*, LO of *Discoaster brouweri*, LO of *Discoaster pentaradiatus*, LO of *Discoaster surculus*, and LO of *Discoaster tamalis*. The FO of *E. huxleyi* was not precisely detected due to poor preservation and dissolution of nannofossils in the underlying strata. We refined the previous calcareous nannofossil biostratigraphy in the SCS by identifying *Gephyrocapsa* species and four evolutionary extinction events of the genus *Discoaster*. The proposed calcareous nannofossil biostratigraphy correlates with those reported in other terrestrial and marine areas/sites and global benthic foraminiferal $\delta^{18}O$ records. The age–depth curves based on nannofossil biostratigraphy indicate a significant increase in the sedimentation rates at the LO of *R. asanoi* (0.91–0.85 Ma). The timing of this increase corresponds to reef expansion in the Ryukyu Islands linked to a stepwise increase in Kuroshio Current intensity. This timing is broadly coeval with a sea surface temperature increase of ~2°C in the northwestern Pacific due to expansion of the Western Pacific Warm Pool towards the north and south subtropical regions. This can be explained by increased weathering and erosion of terrestrial areas in glacial periods and increased rainfall causing higher sediment transport in interglacial periods, which were both linked to Middle Pleistocene Transition-related climatic changes.

Keywords: biostratigraphy, calcareous nannofossil, first occurrence, last occurrence, Ocean Drilling Program, Pliocene–Pleistocene, South China Sea.

1 Introduction

The South China Sea (SCS) is the largest marginal sea in the western Pacific Ocean. The SCS is bounded by the Indochina Block to the west, the Philippine Sea Plate to the east, and the Yangtze Block to the north (Figure 1). The formation of the SCS basin was closely related to the collision between the Indian and Eurasian plates (Sun, 2016). The SCS underwent five stages of tectonic evolution: rift system development (55–50 Ma), seafloor spreading (37–25.5 Ma), subsidence (25 and 5 Ma), closure (10 Ma), and uplift of Taiwan (5–4 Ma; Cullen et al., 2010).

A large number of paleoclimatic (Jiang et al., 2015; Li et al., 2017; Liu et al., 2003), paleoceanographic (Huang et al., 2005; Jian et al., 2000; Li et al., 2006, 2008; Wang et al., 1995), paleoenvironmental (Hu et al., 2002; Sun and Li, 1999; Zhao, 2005), and biostratigraphic studies (Huang, 1997; Li et al., 2004, 2006; Nathan and Leckie, 2003; Su et al., 2004; Wang, 1990) have been carried out in the SCS. Most geological data have been obtained from offshore petroleum exploration wells. In 1999, thick sediment sequences were recovered during Ocean Drilling Program (ODP) Leg 184 in the SCS. These sediments have been subjected to paleoenvironmental, paleoclimatic, and paleoceanographic studies (Huang et al., 2005; Li et al., 2008, 2011). However, there are limited biostratigraphic constraints on the successions recovered from the ODP sites in the SCS, which include planktic foraminiferal biostratigraphy (Li et al., 2005) and calcareous nannofossil biostratigraphy (Su et al., 2004). In a previous study of calcareous nannofossil biostratigraphy at ODP Site 1146 (Su et al., 2004), the sampling resolution was relatively low (~1 m intervals), and some important datums were not detected.

On the northern slope of the SCS, ODP Leg 184 identified three main depositional stages during the late Cenozoic: (1) extremely high sedimentation rates during the Oligocene; (2) lower sedimentation rates and high sediment carbonate contents during the Miocene and early Pliocene; (3) high rates of clastic sediment accumulation since 3 Ma. The high sedimentation rates and widespread carbonate successions in the SCS provide an ideal basis to construct a high-resolution calcareous nannofossil biostratigraphic framework. The aim of this study was to improve the resolution of the calcareous nannofossil biostratigraphy for the SCS.

During the 1970s and 1980s, calcareous nannofossil biostratigraphic zones were proposed for the Mesozoic (Sissingh, 1977) and Cenozoic (e.g., Bukry, 1973, 1975; Martini, 1971; Okada and Bukry, 1980). The Pleistocene zonation proposed by Gartner (1977) included seven biozones for the Caribbean and Pacific basins. Subsequently, Takayama and Sato (1987) identified 12 evolutionary events in the Pleistocene succession recovered during ODP Leg 94 in the North Atlantic. Most recent studies have focused on refining Pleistocene evolutionary events and improving the standard zonation by means of the first and last occurrence datums of age-diagnostic species (Raffi et al., 1993; Rio et al., 1990; Wei, 1993). However, some studies have also considered the beginnings and ends of acme events of certain characteristic taxa (Raffi et al., 2006). Pleistocene calcareous nannofossil datums and their chronostratigraphic framework have been investigated for several decades, and these events have been used to calibrate magnetostratigraphic records (Maiorano et al., 1994; Marino, 1996; Raffi, 2002; Raffi and Rio, 1979; Rio, 1982; Takayama and Sato, 1987) or the astrochronological timescale via oxygen isotope stratigraphy (Flores et al., 2000; Hilgen et al., 2005; Langereis and Hilgen, 1991; Lourens et al., 1992; Raffi, 2002; Raffi et al., 1993, 2006; Sato et al., 2009; Shackleton and Hall, 1989; Shackleton et al., 1990, 1995, 1999; Thierstein et al., 1977; Wei, 1993), thereby providing absolute ages for the datums and showing that the datums are globally synchronous.

The objective of this study was to establish a high-resolution upper Pliocene to Pleistocene calcareous nannofossil biostratigraphy of the SCS, and to correlate it with those in other areas/sites worldwide and the global benthic foraminiferal $\delta^{18}O$ record. Although the previous calcareous nannofossil biostratigraphy of the SCS did not include some significant Pleistocene datums (Su et al., 2004), they are introduced into our biostratigraphy to increase the temporal resolution and improve the accuracy of the new biostratigraphy.

2 Oceanographic Setting

The SCS lies in the tropical region and ranges from the equator to 23°N and from 99° to 121°E. The SCS is connected to the Pacific Ocean through the Luzon Strait (Bashi Strait or Bashi Channel) between Taiwan and Luzon islands (Figure 1). The modern SCS is located in the monsoon regime. Winter monsoons from the north and northeast carry cold and dry winds across the marginal seas to the east of the Eurasian continent (Figure 1; Li et al., 2018). Cold, saline surface waters flow from the East China and Yellow seas southward into the SCS through the Taiwan Strait, forming a counterclockwise gyre in winter (Li et al., 2008). As a result, the winter sea surface temperature (SST) drops to 20–23 °C in the northern SCS and to ~27 °C in the southern SCS (Wang and Li, 2009). During summer, the prevailing southwest monsoon carries warm equatorial Indian Ocean water flowing over the Sunda Shelf into the SCS, resulting in a high and uniform SST (~29 °C). A series of small clockwise gyres (Figure 1) are formed when water flows from the north, especially when western Pacific water flows through the Bashi Strait (Li et al., 2008).

During the Last Glacial Maximum (LGM), the SCS became a semi-isolated basin after losing half of its surface area (>52%) as a result of shelf exposure. The three major shelf areas that emerged during the LGM, the East China Sea Shelf, Sunda Shelf (Great Asian Bank), and Sahul Shelf (Great Australian Bank), have a combined area of 3,900,000 km^2, which is comparable in size to the Indian subcontinent (Wang, 1997). Sea-level falls have greatly altered the configuration and area of the western Pacific marginal seas. Given that the shelf area of the SCS is located mainly in the modern Western Pacific Warm Pool, which is bounded to the west by the 28 °C surface isotherm, the reduction in size of the SCS during the LGM must have profoundly influenced the thermodynamic role exerted by the Global Warm Pool (Prell et al., 1999).

3 Materials and Methods

ODP Leg 184, Site 1146, Hole A is located at 19°27.40′N and 116°16.37′E, at a water depth of 2092 m (Figure 1), which is above the current sill depth of the Bashi Strait (2600 m) in the northern SCS (Shipboard Scientific Party, 2000). Three holes (ODP holes 1146A–C) were drilled at this site. The lithology at this site is mainly nannofossil ooze and clays with varying proportions of biogenic carbonates of early Miocene (*ca.* 19 Ma) to Pleistocene (*ca.* 0.01 Ma) age (Shipboard Scientific Party, 2000). The Pleistocene sediments extend to 201 meters below sea floor (mbsf), and consist of greenish gray nannofossil clay that is relatively enriched in quartz and feldspar, with thin interlayers of volcanic ash and silt-sized quartz in some intervals (Figure 2). The sediments grade downhole into Pliocene clayey nannofossil ooze (201–306 mbsf). The Miocene sediments occur from 306 to 607 mbsf. Samples for this study were collected from the upper Pliocene to Pleistocene interval in ODP Hole 1146A, extending down to 241.92 mbsf with a sampling interval of ~40 cm.

A total of 616 samples were analyzed to establish a high-resolution calcareous nannofossil biostratigraphy (Table S1, Figure 3). The microscope slides were prepared following the conventional method (e.g., Imai et al., 2015, 2020). The slides were observed under a ZEISS Axioskop 2 binocular polarizing microscope (Zeiss, Jena) with an oil immersion objective lens at a magnification of 1500×.

At least 200 nannofossil specimens were identified for each slide to assess the stratigraphic distribution of each species and to correlate species abundance (including presence/absence) to known nannofossil events (i.e., the first occurrence [FO] and last occurrence [LO]). Simultaneously, random observations were repeatedly performed to crosscheck for the presence/absence of age-diagnostic species. Taxonomy of the calcareous nannofossils follows those of Takayama and Sato (1987) and Sato and Takayama (1992).

4 Results

4.1 Preservation

The preservation of calcareous nannofossils is generally moderate to good throughout the studied intervals. However, some of the sampling intervals contain poorly preserved nannofossils and/or are nearly barren. The interval between 101.23 and 162.16 mbsf is characterized by poor preservation of nannofossils (Figure 2). In addition, in some intervals between 33.58 and 70.53 mbsf, above the LO of *Pseudoemiliania lacunosa*, moderate overgrowths and dissolution are apparent. The taphonomic alteration masks part or all of the specimens, making it somewhat difficult to consistently distinguish gephyrocapsid species as well to identify *Emiliania huxleyi*. The intervals of poor preservation are characterized by low abundances of nannofossils; some of these intervals contain large amounts of calcite crystals of unknown origin. The paucity of nannofossils in the intervals 116.25–119.79 and 134.30–140.24 mbsf made it difficult to determine the horizons of some nannofossil events, such as the LO of *Reticulofenestra asanoi* and LO of large *Gephyrocapsa*.

4.2 Nannofossil datums

In ODP Hole 1146A, the upper Pliocene to Pleistocene sediments yielded more than 45 species, varieties, and morphotypes of calcareous nannofossils. The assemblages are characterized by small *Gephyrocapsa* spp., which occur throughout the Pleistocene sediments with a relative abundance of >30%, whereas the upper Pliocene assemblages are dominated by *P. lacunosa* (>15%) and small forms of *Reticulofenestra* species (>20%) in most sample intervals. *Discoaster* spp. occur in the upper Pliocene to lower Pleistocene sediments with a relative abundance of <10%. Other species such as *Calcidiscus leptoporus*, *Rhabdosphaera clavigera*, *Umbilicosphaera sibogae*, *Syracosphaera pulchra*, and *Helicosphaera carteri* occur continuously throughout the studied interval.

A total of 14 calcareous nannofossil datums were identified in the interval of 0–242 mbsf, covering a timespan of *ca.* 2.8 Myr (Tables 1; Figure 3). The FO *of E. huxleyi* occurred at 33.18–33.58 mbsf upwards. However, the actual FO may be lower because dissolution in the interval from 33.58 to 70.53 mbsf made it difficult to identify *E. huxleyi*. The LO of *P. lacunosa* in ODP Hole 1146A was detected at 72.53–72.93 mbsf. Preservation of this species was moderate to good (Figure 4b-1, b-2), except for the interval 101.23–162.16 mbsf, in which calcareous nannofossils were generally poorly preserved. Therefore, the analyzed core is late Pliocene to Pleistocene in age. The LO of *Helicosphaera sellii* and FO and LO of *Helicosphaera inversa* were not detected because these species occurred rarely and sporadically.

We calculated the sedimentation rate based on 12 calcareous nannofossil datums (Table 2). This is because two of the events (FO of *E. huxleyi* and LO of *C. macintyrei*) were not in the correct chronological order. We used the numerical ages assigned by Raffi et al. (2006) and Sato et al. (2012) (Table 2). The age–depth curves indicate a wide range of sedimentation rates from 0.8 to 16.2 cm/kyr. The lowest sedimentation rate (0.8 cm/kyr) occurred between the FO of *Gephyrocapsa caribbeanica* and FO of *Gephyrocapsa oceanica*, whereas the highest sedimentation rate (16.0–16.2 cm/kyr) was obtained from the LO of *P. lacunosa* to the seafloor. The curves reveal an increase in sedimentation rate from ~5 cm/kyr in the interval from the LO of *Discoaster tamalis* to the LO of *R. asanoi* to ~13–14 cm/kyr in the interval of the LO of *R. asanoi* to the seafloor.

5 Discussion

5.1 Datum correlation

The detected calcareous nannofossil datums in this study indicate that the analyzed sedimentary succession can be correlated with the NN16 to NN21 zones of Martini (1971) and the CN12 to CN15 zones of Okada and Bukry (1980), corresponding to the late Pliocene–Pleistocene. Our biostratigraphy is consistent with that established by Su et al. (2004), in terms of the chronological sequence (Figure 3). However, there are differences in several datum depths. Furthermore, we introduced five new calcareous nannofossil datums to refine the biostratigraphy of Su et al. (2004).

The FO of *E. huxleyi* (Figure 4a-1, a-2) was detected at a shallower depth (33.18–33.58 mbsf upwards) in ODP Hole 1146A than reported by Su et al. (2004) (62.21 meter composite depth [mcd]) in ODP Hole 1146B. This difference is due to moderate overgrowth and dissolution of calcareous nannofossils in the interval of 33.58–70.53 mbsf, which suggests that the preservation state of calcareous nannofossils spatially varies even at a single site. Furthermore, the cross-over event between *E. huxleyi* and *G. caribbeanica* (upward decrease in abundance of *G. caribbeanica* and upward increase of *E. huxleyi*) was not clearly observed in ODP Hole 1146A, although it has been recorded in many other sites with a wide range of reported ages of 90–63 ka (Bollmann et al., 1998; Flores et al., 1999; Gartner, 1977; Gradstein et al., 2012; Pujos and Giraudeau, 1993; Raffi et al., 2006; Su et al., 2004; Thierstein et al., 1977; Weaver and Thomson, 1993). Therefore, we consider that the actual FO of this species is likely located between 33.58–70.53 mbsf, which is correlated to Marine Isotope Stage 12 (MIS12)–MIS6 of the benthic foraminifera oxygen isotope record of *Uvigerina peregrina* and *Cibicides wuellerstorfi* at ODP Site 1146 (Clemens and Prell, 2003; hereafter called the BOI stratigraphy) (Figure 5). This interpretation is not inconsistent with the FO of *E. huxleyi* in MIS8 (Thierstein et al., 1977) as confirmed by numerous studies (e.g., Raffi et al., 2006; Sato et al., 2012).

The LO of *P. lacunosa* (Figure 4b-1, b-2) in our study (72.53–72.93 mbsf) was detected ~5.6 m above the depth (78.31 mcd) identified by Su et al. (2004) in ODP Hole 1146C. The difference is probably due to the different sampling resolution and/or slight variations in the sedimentary succession between the holes. In this study, the datum occurs slightly below MIS12 of the BOI stratigraphy. This correlation is in good agreement with other studies (Sato et al., 2009, 2012; Figure 5).

The LO of *R. asanoi* (Figure 4c-1, b-2) was placed at 119.38–119.79 mbsf in ODP Hole 1146A and was detected at a similar depth (117.51 mcd) in ODP Hole 1146C (Su et al., 2004). The datum was correlated to MIS23 of the BOI stratigraphy (Figure 5). This is in good agreement with Raffi et al. (2006), in which this event was also located in MIS23. In addition, our data show a good correlation with the magnetostratigraphy in ODP Hole 1146A, as the event was located below the Brunhes–Matuyama boundary (Lisiecki and Raymo, 2005; Marino et al., 2011; Sato et al., 2012; Figure 3). However, there is a slight difference in the LO of *R. asanoi* between this study and Sato et al. (2009), who correlated this event in the northern Atlantic Ocean to the lowest peak of MIS21. However, the LO of *R. asanoi* has been reported to have occurred in MIS22 (Raffi, 2002; Sato and Takayama, 1992; Wei, 1993).

The FO of *Gephyrocapsa parallela* (Figure 4d-1, d-2) was detected at 126.59–126.99 mbsf in ODP Hole 1146A. This is a bioevent that has been newly introduced to calcareous biostratigraphy in the SCS. This datum was correlated to MIS29 of the BOI stratigraphy (Figure 5), in broad agreement with other deep-sea sites (e.g., MIS30/29 by Marino et al., 2011; MIS 27 by Sato et al., 2009, 2012).

The FO of *R. asanoi* (134.30–134.70 mbsf) was detected ~11 m above the depth (145.52 mcd) identified by Su et al. (2004) in the same hole. This depth discrepancy is mainly due to the difference in species identification, because Su et al. (2004) considered the cutoff size of *R. asanoi* is >5 µm, which is different to our study (>6 µm). In the protologue of *R. asanoi* (Sato and Takayama, 1992), the size of this species is defined as >6.0 µm. This definition has been followed in many studies (e.g., Marino et al., 2003; Raffi, 2002; Sato and Takayama, 1992; Wei, 1993). In this study, the FO of *R. asanoi* was located at the MIS35/34 transition of the BOI stratigraphy. This agrees with the correlation of Sato et al. (2009, 2012; MIS34) and Raffi et al. (2006; MIS34–32) (Figure 5).

The LO and FO of large *Gephyrocapsa* (Figure 4e-1, e-2) are new datums for calcareous biostratigraphy in the SCS. The LO was detected at 140.24–140.64 mbsf, although nannofossils were rare in the interval of 134.30–140.24 mbsf. The FO was placed at 152.84–153.25 mbsf despite the poor to moderate state of preservation of this group. The LO was correlated to MIS37 of the BOI stratigraphy (Figure 5). This broadly agrees with the correlation of Raffi et al. (2006; MIS38), but is slightly older than MIS35 as determined by Sato et al. (2009). Although the FO was correlated to MIS47 of the BOI stratigraphy, the isotopic record does not show clear cyclicity or cannot be reliably correlated with the LR04 stack below ~150 mbsf (i.e., below MIS44). Thus, we do not correlate the calcareous nannofossil biostratigraphy with the BOI stratigraphy below this depth. The FO of large *Gephyrocapsa* was reported to be correlated with MIS47 in some previous studies (e.g., Raffi, 2002; Raffi et al., 2006); however, it has also been correlated with MIS44 (Sato et al., 2009), MIS45 (Flores and Marino, 2002), MIS51–47 (Wei, 1993), and MIS55 (Lourens et al., 1996). Therefore, the FO of large *Gephyrocapsa* is likely to be a diachronous event recorded at variable times in different marine and onland sections.

The FO of *G. oceanica* (Figure 4f-1, f-2), a new datum for calcareous nannofossil biostratigraphy in the SCS, was found at 161.35–161.75 mbsf. This species occurred throughout the Pleistocene succession. However, it was extremely rare in the intervals 126.59–126.99 and 140.24–141.64 mbsf. The datum was correlated to MIS60 in the northern Atlantic Ocean (Sato et al., 2009).

The FO of *G. caribbeanica* (Figure 4g-1, g-2) is also a new datum (161.75–162.16 mbsf) for calcareous nannofossil biostratigraphy in the SCS. This datum corresponds to the FO of medium-sized *Gephyrocapsa* of Su et al. (2004), which was recorded at 177.46 mcd in ODP Hole 1146B (Figure 3). The depth difference of this event is mainly due to taxonomical differences, such as the size criterion used to define this species: 4–6 μm in this study versus 3.5 μm in Su et al. (2004). *G. caribbeanica* follows the same trend as *G. oceanica* and was extremely rare from 126.59–126.99 to 140.24–140.64 mbsf. The magnetostratigraphy of ODP Hole 1146B (Shipboard Scientific Party, 2000) indicates that the FO of medium-sized *Gephyrocapsa* of Su et al. (2004) is located below the Olduvai (C2n) normal subchron. This is inconsistent with the FO of *G. caribbeanica*/medium-sized *Gephyrocapsa* slightly above the subchron in many areas/sites (e.g., Kameo et al., 2020; Marino et al., 2003; Raffi., 2002; Raffi et al., 2006; Sato et al., 2012). The FO of *G. caribbeanica* is located at, or immediately above, the top of the Olduvai subchron (Figure 3), if we extrapolate the magnetostratigraphy in ODP Holes 1146B (160.5–165.8 mbsf) and C (162.3–165.0 mbsf) to the studied hole. Given that the top of the Olduvai subchron is correlated to MIS63 (e.g., Lisiecki and Raymo, 2005), the FO of *G. caribbeanica* is correlated to the same stage (Sato et al., 2012). However, Raffi et al. (2006) reported that this datum is located in MIS61–59 (Figure 5). As the FO of *G. oceanica* and *G. caribbeanica* are very close (161.35–161.75 and 161.75–162.05 mbsf, respectively) and they lie at or immediately above the top of the Olduvai subchron, it is likely that there is a hiatus in the sedimentary record at ~161–166 mbsf.

The LO depth of *C. macintyrei* (Figure 4h) in this study (165.22–165.59 mbsf) is identical to that of Su et al. (2004; 167.46 mcd) in ODP Hole 1146A (Figure 3). The FO of *G. oceanica*, FO of *G. caribbeanica*, and LO of *C. macintyrei* are located in descending order in the studied hole. This contrasts with the LO of *C. macintyrei,* which lies above the FO of *G. oceanica* and FO of *G. caribbeanica* in other areas/sites (e.g., Raffi et al., 2006).

The LO of *Discoaster brouweri* (Figure 4i-1–i-3) detected in this study (179.65–180.05 mbsf) is ~5.6 m above that of Su et al. (2004; 185.46 mcd). This difference can be attributed to variable identification of reworked specimens. Su et al. (2004) identified this datum as the top of the interval where this species showed a significant abundance, and hence it was placed 4 m below our datum. However, we defined this datum as the uppermost horizon of the continuous occurrence of well-preserved specimens (i.e., those with its typical distinguishable characteristics of a concave–convex form as shown in Figure 4i-1–i-3). This datum was found ~15 m below the Olduvai subchron (Figure 3), if the magnetostratigraphy in ODP holes 1146B and C is extrapolated to the studied hole, which is consistent with previous studies. The extinction of *D. brouweri* was placed in MIS76, immediately below the Olduvai subchron, in a recent calcareous nannofossil biostratigraphic study (Sato et al., 2012). Raffi et al. (2006) showed that this event was diachronous from MIS79 to MIS73 (Figure 5).

The LO of *Discoaster pentaradiatus* (Figure 4j-l–j-4) identified in this study (200.89–201.29 mbsf) is ~6.8 m above that of Su et al. (2004; 207.91 mcd in ODP Hole 1146C). The difference in depth is likely due to differences in the identification of reworked specimens as described above, because *D. pentaradiatus* was poorly to moderately preserved and mostly fragmented. *D. pentaradiatus* has been reported to be a low abundance component of Pleistocene nannofossil assemblages. Although its reworked coccoliths are reported to be less common than *D. brouweri*, *Discoaster surculus,* and *Discoaster tamalis* (Chapman and Chepstow-Lusty, 1997), we detected fluctuations in the relatively high abundance of this species (*D. pentaradiatus*) down to the base of the studied interval. The LO of this species has been correlated to the lowermost Matuyama Chron (e.g., Raffi et al., 2006) or slightly above it (Gradstein et al., 2012). However, Wei (1993) and Sato et al. (2012) placed this event in MIS90 and MIS86, respectively. Given there are no magnetostratigraphic data for the studied site, we cannot correlate the LO of *D. pentaradiatus* to any MIS stage.

The LO of *D. surculus* (Figure 4k-1–k-4) was detected at 203.42–203.82 mbsf, which is ~14 m above the LO depth of Su et al. (2004) in ODP Hole 1146B (217.46 mcd; Figure 3). The difference is likely due to the rarity and poor preservation of this species, which makes it difficult to detect its actual LO, as well as differences in the identification of reworked specimens.

Su et al. (2004) placed the LO of *D. surculus* at the Piacenzian/Gelasian boundary (2.58 Ma; Gradstein et al., 2012). However, this datum was correlated to MIS96 (2.44 Ma), located above the Piacenzian/Gelasian boundary in the northern Atlantic Ocean (Sato et al., 2012; Figure 5).

The LO of *D. tamalis* (Figure 4l-1–l-4) is located at 212.92–213.32 mbsf, which is ~11 m above that found by Su et al. (2004) in the same hole (224.11 mcd; Figure 3). This discrepancy is attributed to the difference in the identification of reworked specimens as described for the LO of *D. brouweri*. The LO of *D. tamalis* is found nearly at the top of the Piacenzian, as evidenced by nannofossil biostratigraphic correlations of a number of deep-sea sites and constrained by magnetobiostratigraphy (Raffi et al., 2006; Sato et al., 2012; Wei, 1993). We followed this correlation. This bioevent is broadly correlated with G7 of the LR04 stack (Jatiningrum and Sato, 2017).

5.2 Sedimentation Rate

We constructed age–depth curves for the upper Pliocene to Pleistocene succession in ODP Hole 1146A using the calcareous nannofossil biostratigraphy constrained by the BOI stratigraphy and its correlation with nannofossil biostratigraphy at other areas/sites. The age–depth curves are based on 12 of the 14 nannofossil events. This is because two of the events (FO of *E. huxleyi* and LO of *C. macintyrei*) were not in correct chronological order as described above. We used the numerical ages assigned by Raffi et al. (2006) and Sato et al. (2012) (Table 2; Figure 6). The generated age–depth curves show that sedimentation rates fluctuated in a wide range from 0.8 to 16.2 cm/kyr, with an average of ~7.6 cm/kyr since *ca.* 2.8 Ma.

The two age–depth curves exhibit similar trends, except for the upper Pliocene interval. This is due to a difference in numerical ages for the LO of *D. pentaradiatus* (2.43–2.50 versus 2.24 Ma). The age–depth curves show a marked increase in sedimentation rate from ~5 cm/kyr in the interval from the LO of *D. tamalis* to the LO of *R. asanoi* to ~13–14 cm/kyr in the interval from the LO of *R. asanoi* to the seafloor. The timing of this change in the sedimentation rate broadly corresponds to the timing of reef expansion in the Ryukyu Islands (Iryu et al., 2006; Yamamoto et al., 2006), which can be linked to a stepwise increase in Kuroshio Current intensity related to the magnitude of glacio-eustatic variability through the Middle Pleistocene Transition (Gallagher et al., 2015; Mudelsee and Schulz, 1997). This change is also broadly coeval with the timing of increased SSTs in the northwestern Pacific by ~2˚C in MIS 19 (*ca.* 0.8 Ma), which is considered to be due to the expansion of the Western Pacific Warm Pool towards the north and south subtropical regions (Sakai, 2003). The coeval increases in sedimentation rates offshore of Vietnam and Boso Peninsula, Japan (Sato, 1988; Sato et al., 2008) have been interpreted to reflect climatic changes at the Middle Pleistocene Transition. These changes occurred due to increased weathering and erosion of terrestrial areas in glacial periods and increased rainfall that caused increased sediment transport in interglacial periods. This interpretation also applies to our study, as the Pearl and Red rivers flow into the SCS (Figure 1; Head and Gibbard, 2015; Wan et al., 2010).

6 Conclusions

We have presented a refined calcareous nannofossil biostratigraphy for ODP Site 1146 in the SCS. A total of 14 events from the late Pliocene to Pleistocene spanning *ca.* 2.8 Myr were recognized. They are, in descending order: the FO of *E. huxleyi*, LO of *P. lacunosa*, LO of *R. asanoi*, FO of *G. parallela*, FO of *R. asanoi*, LO of large *Gephyrocapsa*, FO of large *Gephyrocapsa*, FO of *G. oceanica*, FO of *G. caribbeanica*, LO of *C. macintyrei*, LO of *D. brouweri*, LO of *D. pentaradiatus*, LO of *D. surculus*, and LO of *D. tamalis*. The calcareous nannofossil biostratigraphy of this study includes five events involving *Gephyrocapsa* species that were not distinguished in a previous biostratigraphic study at this site (Su et al., 2004).

The biostratigraphic events were correlated to the BOI stratigraphy (Clemens and Prell, 2003) and LR04 stack (Lisiecki and Raymo, 2005). Although some events show discrepancies with previous data, the detected calcareous nannofossil events are broadly consistent with previous records. These discrepancies are caused by differences in sample resolution, species assignment (*R. asanoi* and gephyrocapsid taxa) as well as the poor preservation state in some sample intervals, which hinders the identification of some species such as *E. huxleyi* and *Gephyrocapsa* spp. Furthermore, *Helicosphaera* spp. events were not identified in this study, because *H. inversa* and *H. sellii* occur rarely and sporadically, and thus it was difficult to determine the FO and LO of these taxa.

Age–depth curves were constructed from 12 calcareous nannofossil datums. The age–depth curves indicate a significant increase in the sedimentation rate at the LO of *R. asanoi* (0.91–0.85 Ma). The timing of this increase corresponds to reef expansion in the Ryukyu Islands, which is linked to a stepwise increase in Kuroshio Current intensity. This is broadly coeval with the timing of increased SSTs in the northwestern Pacific due to expansion of the Western Pacific Warm Pool towards the north and south subtropical regions. The coeval increase in sedimentation rates reported from offshore Vietnam and Boso Peninsula, Japan (Sato, 1988; Sato et al., 2008), is interpreted to have resulted from increased weathering and erosion of terrestrial areas in glacial periods and increased rainfall causing increased sediment transport in interglacial periods, which are both linked to Middle Pleistocene Transition-related climatic changes. This interpretation may also explain the increased sedimentation rates in the SCS.

Acknowledgements

This research used samples and data provided by the ODP. Sediment subsampling was performed by the staff of the Kochi Institute for Core Sample Research for supporting IODP operations. This research was supported by The International Joint Graduate Program in Earth and Environmental Sciences (GP-EES), Tohoku University, Japan. The manuscript was significantly improved by the comments and suggestions of T. Irizuki (Associate Editor) and two anonymous reviewers.

References

Bollmann, J., Baumann, K. H., & Thierstein, H. R. (1998). Global dominance of *Gephyrocapsa* coccoliths in the late Pleistocene: Selective dissolution, evolution, or global environmental changes? *Paleoceanography*, *13*, 517–529.

Bukry, D. (1973). Low-latitude coccolith biostratigraphic zonation. In N. T. Edgar, J. B. Saunders, et al. (Eds.), *Initial reports of the Deep Sea Drilling Project, Vol. 15* (pp. 685–703). Washington, D.C.: U. S. Government Printing Office.

Bukry, D. (1975). Coccolith and silicoflagellate stratigraphy, northwestern Pacific Ocean, Deep Sea Drilling Project Leg 32. In R. L. Larson, R. Moberly, et al. (Eds.), *Initial reports of the Deep Sea Drilling Project, Vol. 32* (pp. 677–701). Washington, D.C.: U. S. Government Printing Office.

Chapman, M. R., & Chepstow-Lusty, A. J. (1997). Late Pliocene climatic change and the global extinction of the discoasters: an independent assessment using oxygen isotope records.

Palaeogeography, Palaeoclimatology, Palaeoecology, *134*, 109–125.

Clemens, S. C., & Prell, W. L. (2003). *3. Data report: oxygen and carbon isotopes from Site 1146, northern South China Sea*. In W. L. Prell, P. Wang, P. Blum, D. K. Rea, & S. C. Clemen (Eds.), *Proceedings of the Ocean Drilling Program, scientific results, Vol. 184*. College Station, Texas: Ocean Drilling Program. Retrieved from https://doi.org/10.2973/odp.proc.sr.184.214.2003

Cullen, A., Reemst, P., Henstra, G., Gozzard, S., & Ray, A. (2010). Rifting of the South China Sea: new perspectives. *Petroleum Geoscience*, *1*, 273–282.

Flores, J. A., Gersonde, R. R., Sierro, F. J., & Niebler, H. S. (2000). Southern ocean Pleistocene calcareous nannofossil events: Calibration with isotope and geomagnetic stratigraphies. *Marine Micropaleontology*, *40*, 377–402.

Flores, José Abel, Gersonde, R., & Sierro, F. J. (1999). Pleistocene fluctuations in the Agulhas Current Retroflection based on the calcareous plankton record. *Marine Micropaleontology*, *37*, 1–22.

Flores, José Abel, & Marino, M. (2002). Pleistocene calcareous nannofossil stratigraphy for ODP Leg 177 (Atlantic sector of the Southern Ocean). *Marine Micropaleontology*, *45*, 191–224.

Gallagher, S. J., Kitamura, A., Iryu, Y., Itaki, T., Koizumi, I., & Hoiles, P. W. (2015). The Pliocene to recent history of the Kuroshio and Tsushima Currents: a multi-proxy approach. *Progress in Earth and Planetary Science*, *2*, 17. doi: 10.1186/s40645-015-0045-6

Gartner, S. (1977). Calcareous nannofossil biostratigraphy and revised zonation of the Pleistocene. *Marine Micropaleontology*, *2*, 1–25.

Gradstein, F. M., Ogg, J. G., Schmitz, M., & Ogg, G. (2012). *The geologic time scale 2012* (Vol. 1 and 2). Amsterdam, The Netherlands: Elsevier.

Head, M. J., & Gibbard, P. L. (2015). Early–Middle Pleistocene transitions: linking terrestrial and marine realms.*Quaternary International*, *389*, 7–46.

Hilgen, F., Abdul Aziz, H., Bice, D., Iaccarino, S., Krijgsman, W., Kuiper, K., Montanari, A., Raffi, I., Turco, E., Zachariasse, W. J. (2005). The Global Boundary Stratotype Section and Point (GSSP) of the Tortonian Stage (Upper Miocene) at Monte Dei Corvi. *Episodes*, *28*, 6–17.

Hu, J., Jia, G., Fang, D., Zhang, G., Fu, J., & Wang, P. (2002). Biological markers and their carbon isotopes as an approach to the paleoenvironmental reconstruction of Nansha area, South China Sea, during the last 30 ka. *Organic Geochemistry*, *33*, 1197–1204.

Huang, B., Jian, Z., & Wang, P. (2005). Paleoceanographic evolution recorded in the northern South China Sea since 4 Ma. *Science in China, Series D: Earth Sciences*, *48*, 2166–2173.

Huang, L. (1997). Calcareous nannofossil biostratigraphy in the Pearl River Mouth Basin, South China Sea, and Neogene reticulofenestrid coccoliths size distribution pattern. *Marine Micropaleontology*, *32*, 31–57.

Imai, R., Farida, M., Sato, T., & Iryu, Y. (2015). Evidence for eutrophication in the northwestern Pacific and eastern Indian oceans during the Miocene to Pleistocene based on the nannofossil accumulation rate, *Discoaster* abundance, and coccolith size distribution of *Reticulofenestra*. *Marine Micropaleontology*, *116*, 15–27.

Imai, R., Sato, T., Chiyonobu, S., & Iryu, Y. (2020). Reconstruction of Miocene to Pleistocene sea-surface conditions in the eastern Indian Ocean on the basis of calcareous nannofossil assemblages from ODP Hole 757B. *Island Arc*, *29*, e12373.

Iryu, Y., Matsuda, H., Machiyama, H., Piller, W. E., Quinn, T. M., & Mutti, M. (2006). Introductory perspective on the COREF Project. *Island Arc*, *15*, 393–406.

Jatiningrum, R. S., & Sato, T. (2017). Sea-surface dynamics changes in the subpolar North Atlantic Ocean (IODP Site U1314) during late Pliocene climate transition based on calcareous nannofossil observation. *Open Journal of Geology*, *7*, 1538.

Jian, Z., Wang, P., Chen, M.-P., Li, B., Zhao, Q., Bühring, C., Laj, C., Lin, H.-L., Pflaumann, U., Bian, R., & Cheng, X. (2000). Foraminiferal response to major Pleistocene paleoceanographic changes in the southern South China Sea. *Paleoceanography*, *15*, 229–243.

Jiang, D., Yu, G., Zhao, P., Chen, X., Liu, J., Liu, X., Wang, S., Zhang, Z., Yu, Y., Li, Y., Jin, L., Xu, Y., Ju, L., Zhou, T., & Yan, X. (2015). Paleoclimate modeling in China: A review. *Advances in Atmospheric Sciences*, *32*, 250–275.

Kameo, K., Kubota, Y., Haneda, Y., Suganuma, Y., & Okada, M. (2020). Calcareous nannofossil biostratigraphy of the Lower–Middle Pleistocene boundary of the GSSP, Chiba composite section in the Kokumoto Formation, Kazusa Group, central Japan, and implications for sea-surface environmental changes. *Progress in Earth and Planetary Science*, *7*, 36. doi: 10.1186/s40645-020-00355-x

Langereis, C. G., & Hilgen, F. J. (1991). The Rossello composite: a Mediterranean and global reference section for the Early to early Late Pliocene. *Earth and Planetary Science Letters*, *104*, 211–225.

Li, B., Jian, Z., Li, Q., Tian, J., & Wang, P. (2005). Paleoceanography of the South China Sea since the middle Miocene: evidence from planktonic foraminifera. *Marine Micropaleontology*, *54*, 49–62.

Li, L., Li, Q., Tian, J., Wang, P., Wang, H., & Liu, Z. (2011). A 4-Ma record of thermal evolution in the tropical western Pacific and its implications on climate change. *Earth and Planetary Science Letters*, *309*, 10–20.

Li, M., Ouyang, T., Roberts, A. P., Heslop, D., Zhu, Z., Zhao, X., Tian,C., Peng, S., Zhong, H., Peng, X. & Qiu, Y. (2018). Influence of sea level change and centennial East Asian monsoon variations on northern South China Sea sediments over the past 36 kyr. *Geochemistry, Geophysics, Geosystems*, *19*, 1674–1689.

Li, Q., Jian, Z., & Li, B. (2004). Oligocene–Miocene planktonic foraminifer biostratigraphy, Site 1148, northern South China Sea. In W. L. Prell, P. Wang, P. Blum, D. K. Rea, & S. C. Clemens (Eds.), *Proceedings of the Ocean Drilling Program, scientific results, Vol. 184*. College Station, Texas: Ocean Drilling Program. Retrieved from https://doi.org/10.2973/odp.proc.sr.184.220.2004

Li, Q., Wang, P., Zhao, Q., Shao, L., Zhong, G., Tian, J., Cheng, X., & Su, X. (2006). A 33 Ma lithostratigraphic record of tectonic and paleoceanographic evolution of the South China Sea. *Marine Geology*, *230*, 217–235.

Li, Q., Wang, P., Zhao, Q., Tian, J., Cheng, X., Jian, Z., Zhong, G., & Chen, M. (2008). Paleoceanography of the mid-Pleistocene South China Sea. *Quaternary Science Reviews*, *27*, 1217–1233.

Li, Z., Pospelova, V., Liu, L., Zhou, R., & Song, B. (2017). High-resolution palynological record of Holocene climatic and oceanographic changes in the northern South China Sea. *Palaeogeography, Palaeoclimatology, Palaeoecology*, *483*, 94–124.

Lisiecki, L. E., & Raymo, M. E. (2005). A Pliocene-Pleistocene stack of 57 globally distributed benthic δ 18O records. *Paleoceanography*, *20*, 1–17.

Liu, Z., Trentesaux, A., Clemens, S. C., Colin, C., Wang, P., Huang, B., & Boulay, S. (2003). Clay mineral assemblages in the northern South China Sea: implications for East Asian monsoon evolution over the past 2 million years. *Marine Geology*, *201*, 133–146.

Lourens, L. J., Hilgen, F. J., Gudjonsson, L., & Zachariasse, W. J. (1992). Late Pliocene to early Pleistocene astronomically forced sea surface productivity and temperature variations in the Mediterranean. *Marine Micropaleontology*, *19*, 49–78.

Lourens, L. J., Hilgen, F. J., Raffi, I., & Vergnaud-Grazzini, C. (1996). Early Pleistocene chronology of the Vrica section (Calabria, Italy). *Paleoceanography*, *11*, 797–812.

Maiorano, P., Marino, M., & Monechi, S. (1994). Pleistocene calcareous nannofossil high resolution biostratigraphy of Site 577, Northwestern Pacific Ocean. *Palaeopelagos*, *4*, 119–127.

Marino, M. (1996). Quantitative calcareous nannofossil biostratigraphy of the lower–middle Pleistocene Montalbano Jonico section (southern Italy). *Palaeopelagos*, *6*, 347–360.

Marino, M., Maiorano, P., & Flower, B. P. (2011). Calcareous nannofossil changes during the Mid-Pleistocene Revolution: paleoecologic and paleoceanographic evidence from North Atlantic Site 980/981. *Palaeogeography, Palaeoclimatology, Palaeoecology*, *306*, 58–69.

Marino, M., Maiorano, P., & Monechi, S. (2003). Quantitative Pleistocene calcareous nannofossil biostratigraphy of Leg 86, Site 577 (Shatsky Rise, NW Pacific Ocean). *Journal of Nannoplankton Research*, *25*, 25–37.

Martini, E. (1971). Standard Tertiary and Quaternary calcareous nannoplankton zonation. *Proc. II Planktonic Conference, Roma 1970, Roma, Tecnoscienza*, *2*, 739–785.

Matsuoka, H., & Okada, H. (1989). Quantitative analysis of Quaternary nannoplankton in the subtropical northwestern Pacific Ocean. *Marine Micropaleontology*, *14*, 97–118.

Mudelsee, M., & Schulz, M. (1997). The mid-Pleistocene climate transition: onset of 100 ka cycle lags ice volume build-up by 280 ka. *Earth and Planetary Science Letters*, *151*, 117–123.

Nathan, S. A., & Leckie, R. M. (2003). Miocene planktonic foraminiferal biostratigraphy of sites 1143 and 1146, ODP Leg 184, South China Sea. In W. L. Prell, P. Wang, P. Blum, D. K. Rea, & S. C. Clemens (Eds.), *Proceedings of the Ocean Drilling Program, scientific results, Vol. 184*. College Station, Texas: Ocean Drilling Program. Retrieved from https://doi.org/10.2973/odp.proc.sr.184.219.2003

Okada, H., & Bukry, D. (1980). Supplementary modification and introduction of code numbers to the low-latitude coccolith biostratigraphic zonation (Bukry, 1973; 1975). *Marine*

Micropaleontology, *5*, 321–325.

Prell, W. L., Wang, P., & Blum, P. (1999). *Ocean Drilling Program Leg 184 preliminary report: South China Sea.* College Station, Texas: Ocean Drilling Program.

Pujos, A., & Giraudeau, J. (1993). Distribution of Noelaerhabdaceae (calcareous nannofossils) in the upper and middle Quaternary of the Atlantic and Pacific oceans. *Oceanologica Acta*, *16*, 349–362.

Raffi, I., (2002). Revision of the early-middle pleistocene calcareous biochronology (1.75–0.85 Ma). *Marine Micropaleontology*, *45*, 25–55.

Raffi, I., Backman, J., Domenico, R. & Shackleton, N. J. (1993). Plio-Pleistocene nannofossil biostratigraphy and calibration to oxygen isotope stratigraphies from Deep Sea Drilling Project Site 607 and Ocean Drilling Program Site 677. *Paleoceanography*, *8*, 387–408.

Raffi, I., Backman, J., Fornaciari, E., Pälike, H., Rio, D., Lourens, L., & Hilgen, F. (2006). A review of calcareous nannofossil astrobiochronology encompassing the past 25 million years. *Quaternary Science Reviews*, *25*, 3113–3137.

Raffi, I., & Rio, D. (1979). Calcareous nannofossil biostratigraphy of DSDP Site 132—Leg 13 (Tyrrhenian Sea-Western Mediterranean). *Rivista Italiana Di Paleontologia e Stratigrafia*, *85*, 127–172.

Rio, D. (1982). The fossil distribution of coccolithophore genus *Gephyrocapsa* Kamptner and related Plio-Pleistocene chronostratigraphic problems. In W. L. Prell, J. V. Gardner, et al., (Eds.), *Initial reports of the Deep Sea Drilling Project, Vol. 68* (pp. 325–343). Washington: U. S.Government Printing Office.

Rio, D., Raffi, I., & Villa. G. (1990). Pliocene–Pleistocene calcareous nannofossil distribution patterns in the western Mediterranean. In K. A. Kastens, J. Mascle, et al. (Eds.), *Proceedings of the Ocean Drilling Program, scientific results, Vol. 107* (pp. 117–121). College Station, Texas: Ocean Drilling Program.

Sakai, S. (2003). Shallow-water carbonates record marginal to open ocean Quaternary paleoceanographic evolution. *Paleoceanography*, *18*, 1–10.

Sato, T. (1988). Calcareous nannofossil zones of the Quaternary. *Memoir of the Geological Society of Japan*, *30*, 205–217.

Sato, T., Chiyonobu, S., & Farida, M. (2012). Terminal Neogene events and beginning of the Quaternary climate system based on calcareous nannofossils. *Journal of the Geological*

Society of Japan, *118*, 87–96 (in Japanese with English abstract).

Sato, T., Chiyonobu, S., & Hodell, D. A. (2009). Data report: Quaternary calcareous nannofossil datums and biochronology in the North Atlantic Ocean, IODP Site U1308. In J. E. T. Channell, T. Kanamatsu, T. Sato, R. Stein, C. A. Alvarez Zarikian, M. J. Malone, & the Expedition 303/306 Scientists (Eds.), *Proceeding of the Integrated Ocean Drilling Program, Vol. 303/306*. College Station, Texas : Integrated Ocean Drilling Program Management International, Inc. Retrieved from https://doi.org/10.2204/iodp.proc.303306.210.2009

Sato, T., Hasegawa, S., Yamazaki, M., & Nakagawa, H. (2008). Paleoenvironmental significance of unconfirmity in the Pleistocece succession off Vietnam. *Abstract , 2008 Technical Meeting of the Japanese Association for Petroleum Technology*, 8.

Sato, T., & Takayama, T. (1992). A stratigraphically significant new species of the calcareous nannofossil *Reticulofenestra asanoi*. In K. Ishizaki, & T. Saito (Eds.), *Centenary of Japanese micropaleontology* (pp. 457–460). Tokyo, Japan: Terra Scientific Publishing Co.

Shackleton, N. J., Berger, A., & Peltier, W. R. (1990). An alternative astronomical calibration of the lower Pleistocene timescale based on ODP Site 677. *Transactions of the Royal Society of Edinburgh: Earth Sciences*, *81*, 251–261.

Shackleton, N. J., Crowhurst, S. J., Weedon, G. P., & Laskar, J. (1999). Astronomical calibration of Oligocene--Miocene time. *Philosophical Transactions of the Royal Society of London. Series A: Mathematical, Physical and Engineering Sciences*, *357*, 1907–1929.

Shackleton, N. J., & Hall, M. A. (1989). Stable isotope history of the Pleistocene at ODP Site 677. In K. Becker, H. Sakai, et al. (Eds.), *Proceedings of the Ocean Drilling Program, scientific results, Vol. 111* (pp. 295–316). College Station, Texas: Ocean Drilling Program.

Shackleton, N.J., Hall, M.A., & Pate, D. (1995). Pliocene stable isotope stratigraphy of site 846. In N. G. Pisias, L. A. Mayer, T. R. Janecek, A. Palmer-Julson, & T. H. van Andel, (Eds.), *Proceedings of the Ocean Drilling Program, scientific results, Vol. 138* (pp. 337–355). College Station, Texas: Ocean Drilling Program.

Shipboard Scienfic Party (2000). 7. Site1146. In P. Wang, W. L. Prell, P. Blum et al., *Proceedings of the Ocean Drilling Program, initial reports, Vol. 184*. College Station, Texas: Ocean Drilling Program. Retrieved from https://doi.org/10.2973/odp.proc.ir.184.107.2000

Sissingh, W. (1977). Biostratigraphy of cretaceous nannoplankton biostratigraphy of Cretaceous nannoplankton, with appendix by Prins, B. & Sissingh, W. *Geologie en Mijnbouw, 56*, 37–65.

Su, X., Xu, Y., & Tu, Q. (2004). Early Oligocene-Pleistocene calcareous nannofossil biostratigraphy of the northern South China Sea (Leg 184, Sites 1146-1148). In W. L. Prell, P. Wang, P. Blum, D. K. Rea, & S. C. Clemens (Eds.), *Proceedings of the Ocean Drilling Program, scientific results, Vol. 184*. College Station, Texas: Ocean Drilling Program. Retrieved from https://doi.org/10.2973/odp.proc.sr.184.224.2004

Sun, W. (2016). Initiation and evolution of the South China Sea: an overview. *Acta Geochimica*, *35*, 215–225.

Sun, X., & Li, X. (1999). A pollen record of the last 37 ka in deep sea core 17940 from the northern slope of the South China Sea. *Marine Geology*, *156*, 227–244.

Takayama, T., & Sato, T. (1987). Coccolith biostratigraphy of the North Atlantic Ocean, Deep Sea Drilling Project Leg 94. In W. E. Ruddiman, R. B. Kidd, E. Thomas, et al., (Eds.), *Initial reports of the Deep Sea Drilling Project, Vol. 94* (pp. 651–702). Washington, D.C.: U. S. Government Printing Office.

Thierstein, H. R., Geitzenauer, K. R., Molfino, B., & Shackleton, N. J. (1977). Global synchroneity of late Quaternary coccolith datum levels Validation by oxygen isotopes. *Geology*, *5*, 400–404.

Wan, S., Li, A., Clift, P. D., Wu, S., Xu, K., & Li, T. (2010). Increased contribution of terrigenous supply from Taiwan to the northern South China Sea since 3 Ma. *Marine Geology*, *278*, 115–121.

Wang, P. (1990). Neogene stratigraphy and paleoenvironments of China. *Palaeogeography, Palaeoclimatology, Palaeoecology*, *77*, 315–334.

Wang, P. (1997). Late Cenozoic environmental evolution in China: marine factors and records. In N. G. Jablonski (Ed.), *Proceedings of the 4th International Conference on the Evolution of the East Asian Environment. Hong Kong, 3–7 January 1995* (pp. 264–274). Hong Kong: The University of Hong Kong.

Wang, P., & Li, Q.（Eds.）(2009). *The South China Sea: paleoceanography and sedimentology. Developments in paleoenvironmental research, vol 13.* Berlin, Germany: Springer.

Wang, P., Prell, W. L., Blum, P., Arnold, E. M., Bühring, C. J., Chen, M.-P.,…Wang, L. (2000). *Proceedings of the Ocean Drilling Program, initial reports (Vol. 184)*. College Station, TX:

Ocean Drilling Program.

Wang, P., Wang, L., Bian, Y., & Jian, Z. (1995). Late Quaternary paleoceanography of the South China Sea: surface circulation and carbonate cycles. *Marine Geology*, *127*(1–4), 145–165.

Weaver, P. P. E., & Thomson, J. (1993). Calculating erosion by deep-sea turbidity currents during initiation and flow. *Nature*, *364*, 136.

Wei, W. (1993). Calibration of upper Pliocene–lower Pleistocene nannofossil events with oxygen isotope stratigraphy. *Paleoceanography*, *8*, 85–99.

Yamamoto, K., Iryu, Y., Sato, T., Chiyonobu, S., Sagae, K., & Abe, E. (2006). Responses of coral reefs to increased amplitude of sea-level changes at the Mid-Pleistocene Climate Transition. *Palaeogeography, Palaeoclimatology, Palaeoecology*, *241*, 160–175.

Zhao, Q. (2005). Late Cainozoic ostracod faunas and paleoenvironmental changes at ODP Site 1148, South China Sea. *Marine Micropaleontology*, *54*, 27–47.

Table and Figure Captions

Table 1 Depth at which calcareous nannofossil bioevents were detected in ODP Hole 1146A

Table 2 Calculated sedimentation rates based on calcareous nannofossil bioevents in ODP Hole 1146A

Figure 1 Map of the South China Sea showing the location of ODP Site 1146. The directions of the surface currents and East Asia Monsoon are also shown (modified from Li et al., 2018).

Figure 2 The upper Pliocene–Pleistocene calcareous nannofossil biostratigraphy in ODP Hole 1146A in the South China Sea. Lithological data are from Wang et al. (2000).

Figure 3 Calcareous nannofossil biostratigraphy in ODP Hole1146A established in this study compared with that of Su et al. (2004), biostratigraphic schemes of Martini (1971) and Okada and Bukry (1980), and magnetostratigraphic chrons/subchrons at ODP Site 1146. The superscript letters (A–C) denote ODP 1146 holes A–C, respectively. J = Jaramillo; O = Olduvai.

Figure 4 Photomicrographs of calcareous nannofossils from ODP Hole 1146A. The scale bars are 5 µm in length. a-1, a-2, *Emiliania huxleyi*; b-1, b-2, *Pseudoemiliania lacunosa*; c-1–c-4, *Reticulofenestra asanoi*; d-1, d-2, *Gephyrocapsa parallela*; e-1, e-2, large *Gephyrocapsa* spp.; f-1, f-2, *Gephyrocapsa oceanica*; g-1, g-2, *Gephyrocapsa caribbeanica*; h, *Calcidiscus macintyrei*, i-1–i-3, *Discoaster brouweri*; j-1–j-4, *Discoaster pentaradiatus*; k-1–k-4, *Discoaster surculus*; l-1–l-4, *Discoaster tamalis.*

Figure 5 Correlation of the calcareous nannofossil bioevents in the South China Sea (this study) with those of Raffi et al. (2006) and Sato et al. (2012), and compared with the benthic oxygen isotope stratigraphy (BOI) in the South China Sea (Clemence and Prell, 2003) and LR04 stack (Lisiecki and Raymo, 2005). UI = interval in which the BOI stratigraphy does not necessarily show clear cyclicity, preventing reliable correlation with the LR04 stack.

Figure 6 Age–depth plots for the upper Pliocene to Pleistocene succession in the South China Sea, based on calcareous nannofossil datums. Red circles indicate the plots based on the ages of Sato et al. (2012). Green and blue circles indicate the plots based on the ages assigned by Raffi et al. (2006). For the legend see Fig. 2.

Supporting Information

Table S1 Stratigraphic distribution of age-diagnostic calcareous nannofossils in ODP Hole 1146A.

Table 1 Depth at which calcareous nannofossil bioevents were detected in ODP Hole 1146A

BIOEVENT	Top depth (mbsf)	Bottom depth (mbsf)	Sample source
FO *Emiliania huxleyi*	33.18	70.53	U1146A-5H-1 W, 78.0–79.0 cm
LO *Pseudoemiliania lacunosa*	72.53	72.93	U1146A-9H-2 W, 103.0–104.0 cm
LO *Reticulofenestra asanoi*	119.38	119.79	U1146A-14H-2 W, 119.0–120.0 cm
FO *Gephyrocapsa parallela*	126.59	126.99	U1146A-14H-6 W, 79.0–80.0 cm
FO *Reticulofenestra asanoi*	134.30	134.70	U1146A-14H-2 W, 39.0–40.0 cm
LO large *Gephyrocapsa* spp.	140.24	140.64	U1146A-16H-3 W, 114.0–115.0 cm
FO large *Gephyrocapsa* spp.	152.84	153.25	U1146A-17H-5 W, 4.0–5.0 cm
FO *Gephyrocapsa oceanica*	161.35	161.75	U1146A-18H-4 W, 95.0–96.0 cm
FO *Gephyrocapsa caribbeanica*	161.75	162.16	U1146A-18H-4 W, 135.0–136.0 cm
LO *Calcidiscus macintyrei*	165.22	165.59	U1146A-20H-2 W, 115.0–117.0 cm
LO *Discoaster brouweri*	179.65	180.05	U1146A-20H-4 W, 65.0–66.0 cm
LO *Discoaster pentaradiatus*	200.89	201.29	U1146A-22X-5 W, 139.0–140.0 cm
LO *Discoaster surculus*	203.42	203.82	U1146A-23X-1 W, 82.0–83.0 cm
LO *Discoaster tamalis*	212.92	213.32	U1146A-24X-1 W, 62.0–63.0 cm

Table 2 Calculated sedimentation rates based on calcareous nannofossil bioevents in ODP Hole 1146A

BIOEVENT	Top depth (mbsf)	Bottom depth (mbsf)	Age (Ma) Sato et al. (2012)	Sedimentation rate (cm/kyr)	Age (Ma) Raffi et al. (2006)	Sedimentation rate (cm/kyr)*
				16.2		16.0
LO *Pseudoemiliania lacunosa*	72.53	72.93	0.45		0.44–0.47	
				11.7		10.3
LO *Reticulofenestra asanoi*	119.38	119.79	0.85		0.91	
				5.1		8.0
FO *Gephyrocapsa parallela*	126.59	126.99	0.99		0.96–1.04	
				5.5		7.3
FO *Reticulofenestra asanoi*	134.30	134.70	1.13		1.08–1.13	
				11.9		4.2
LO large *Gephyrocapsa* spp.	140.24	140.64	1.18		1.24–1.25	
				6.0		5.9
FO large *Gephyrocapsa* spp.	152.84	153.25	1.39		1.46	
				2.7		
FO *Gephyrocapsa oceanica*	161.35	161.75	1.71			3.7
				0.8		
FO *Gephyrocapsa caribbeanica*	161.75	162.16	1.76		1.67–1.73	
				7.8		6.2
LO *Discoaster brouweri*	179.65	180.05	1.99		1.92–2.06	
				8.5		4.5
LO *Discoaster pentaradiatus*	200.89	201.29	2.24		2.43–2.50	
				1.3		5.6
LO *Discoaster surculus*	203.42	203.82	2.44		2.49–2.53	
				3.1		2.9
LO *Discoaster tamalis*	212.92	213.32	2.75		2.81–2.86	

* Calculated based on mid values of the chronological ranges for the datums gived by Raffi et al. (2006).

Emanuel et al.
Figure 1

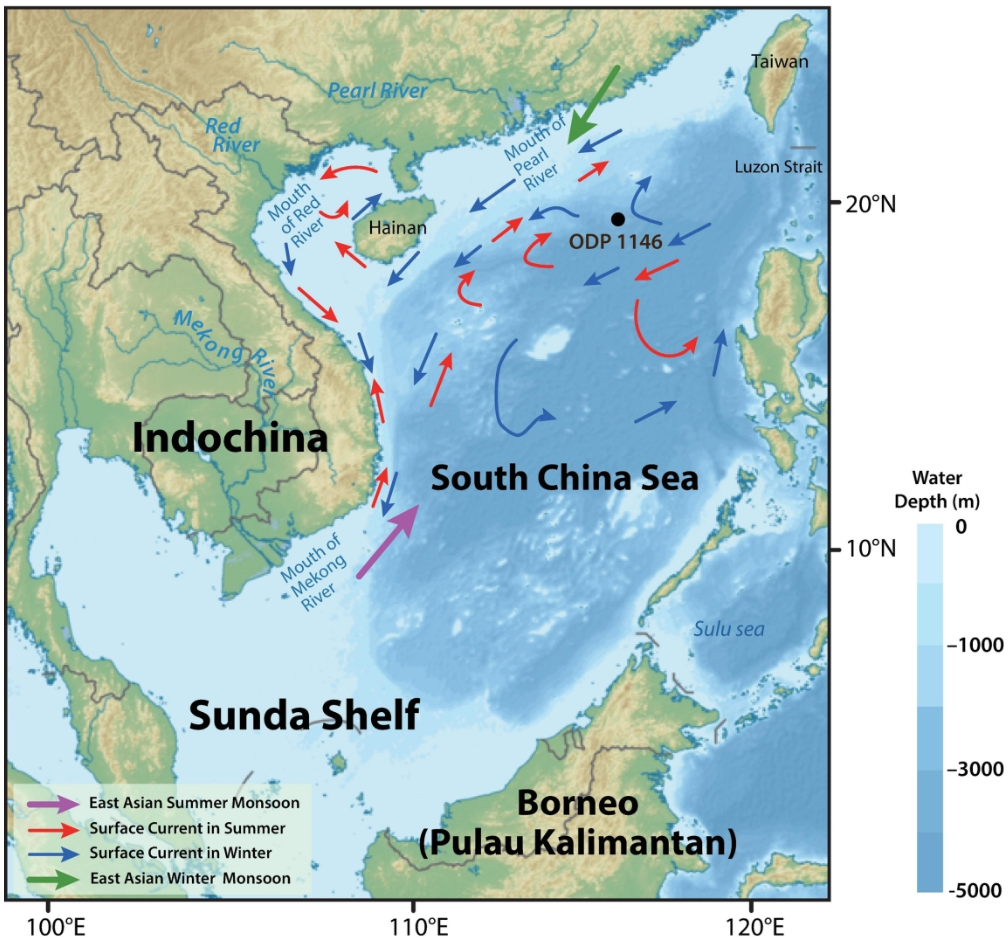

Figure 1 Map of the South China Sea showing the location of ODP Site 1146. The directions of the surface currents and East Asia Monsoon are also shown (modified from Li et al., 2018).

177x183mm (300 x 300 DPI)

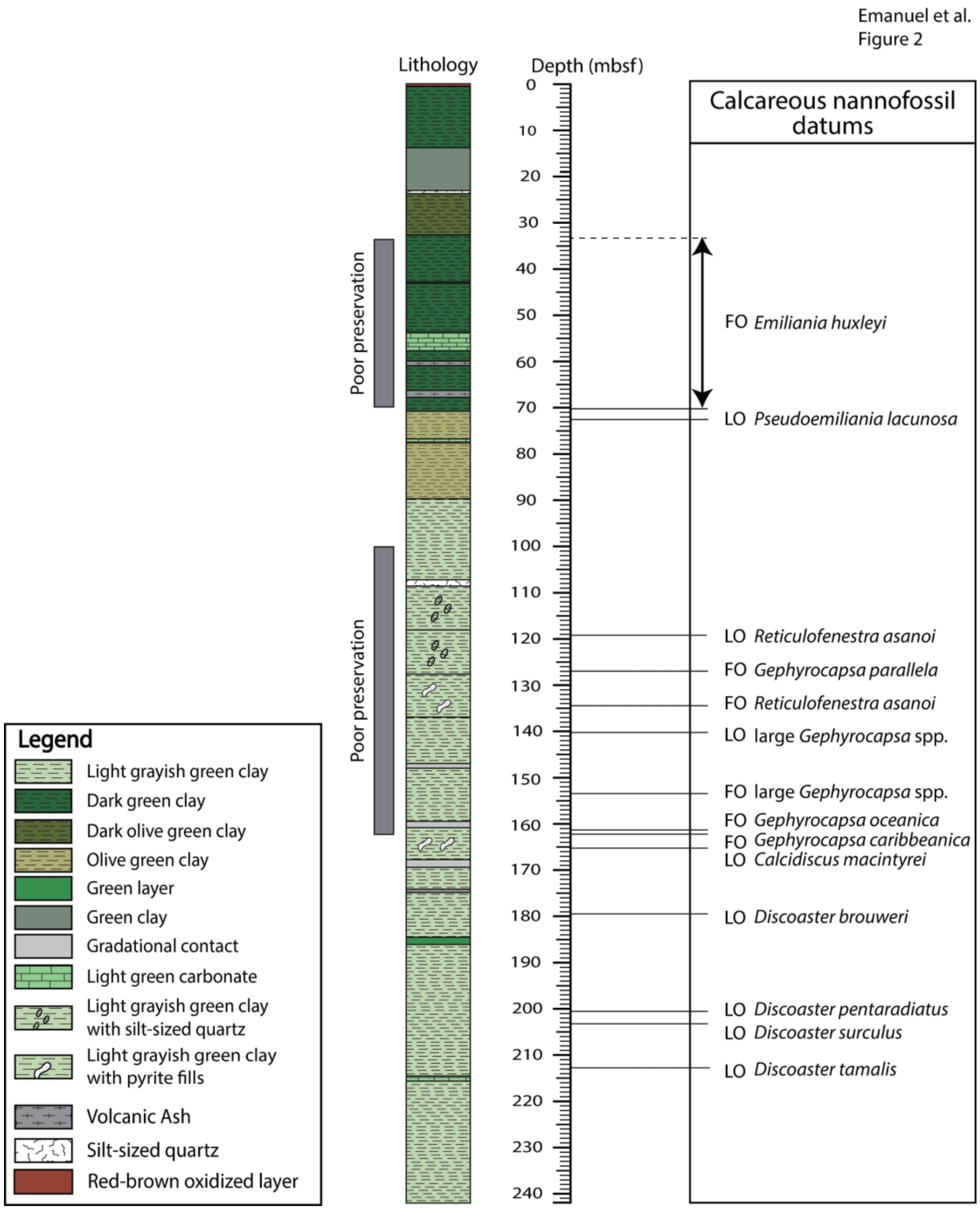

Figure 2 The upper Pliocene–Pleistocene calcareous nannofossil biostratigraphy in ODP Hole 1146A in the South China Sea. Lithological data are from Wang et al. (2000).

176x217mm (300 x 300 DPI)

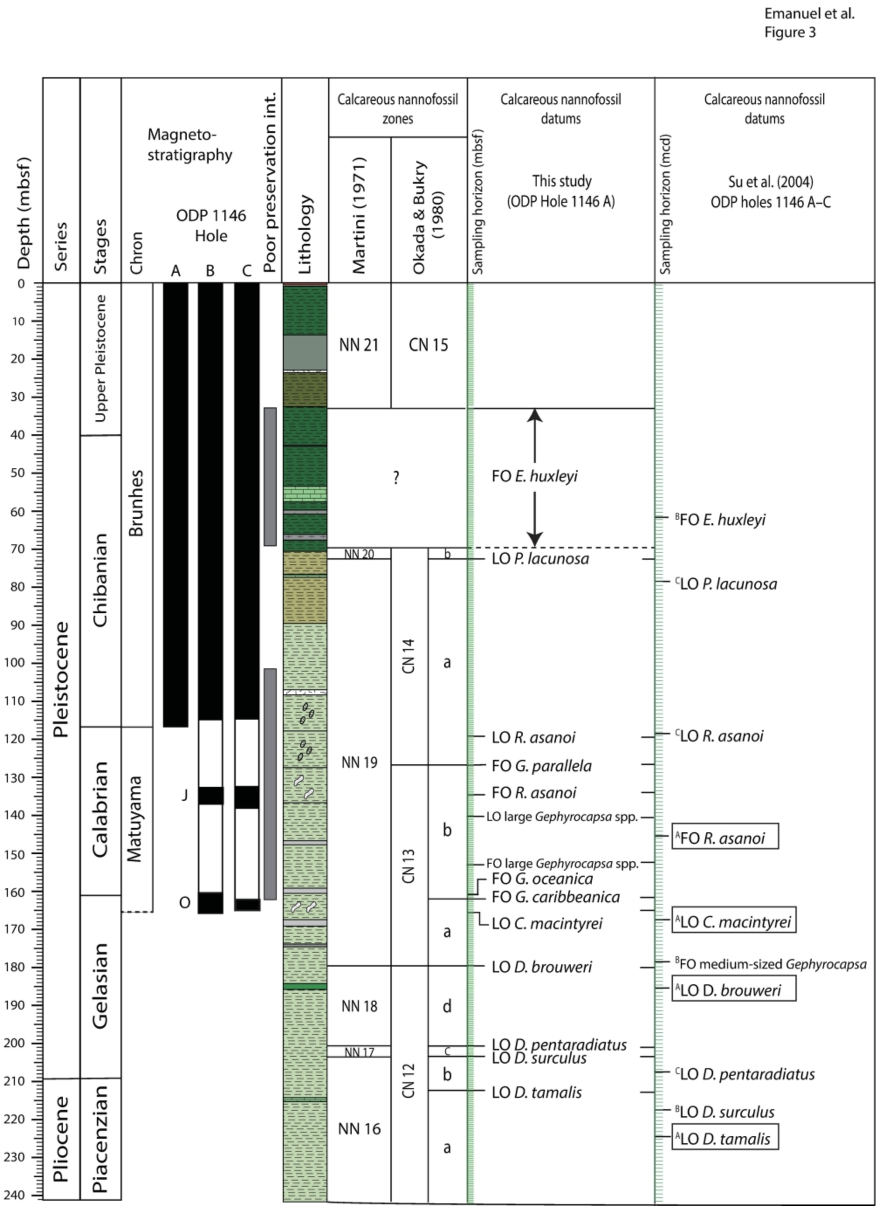

Figure 3 Calcareous nannofossil biostratigraphy in ODP Hole1146A established in this study compared with that of Su et al. (2004), biostratigraphic schemes of Martini (1971) and Okada and Bukry (1980), and magnetostratigraphic chrons/subchrons at ODP Site 1146. The superscript letters (A–C) denote ODP 1146 holes A–C, respectively. J = Jaramillo; O = Olduvai.

200x274mm (300 x 300 DPI)

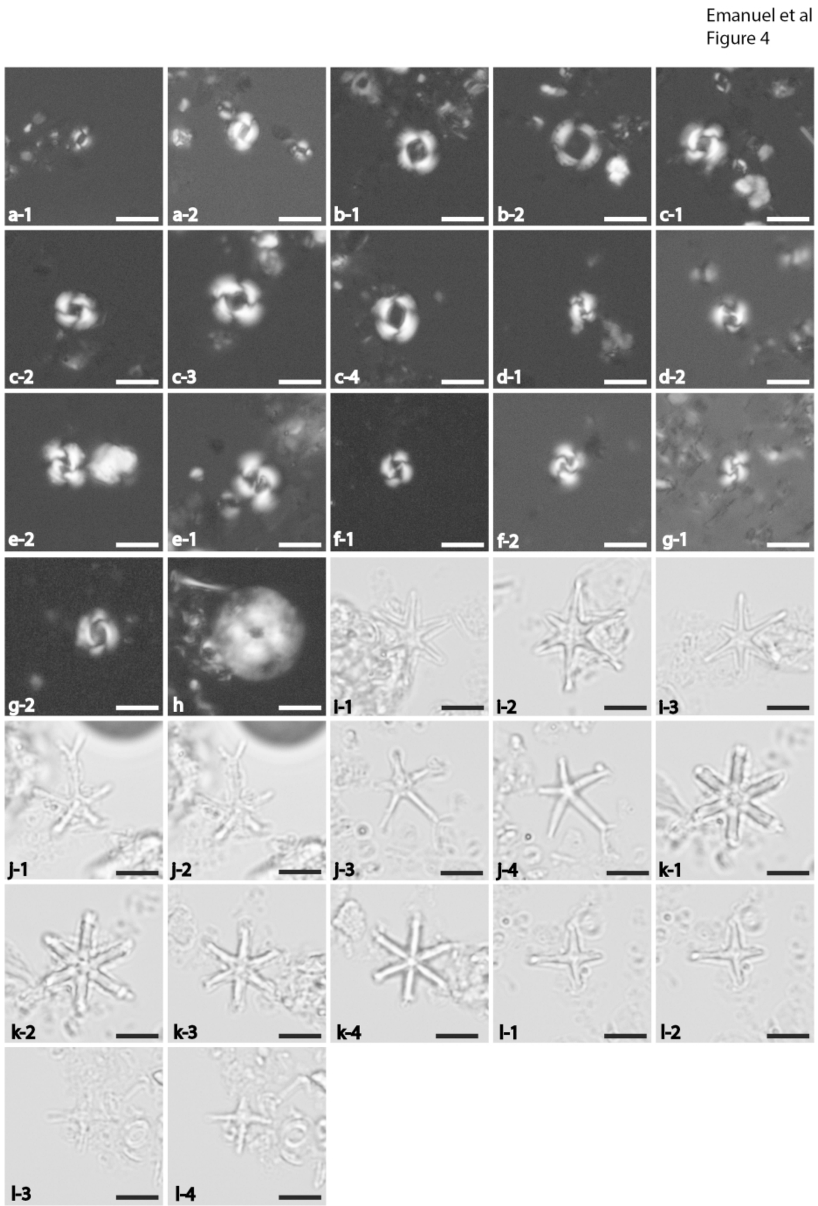

Figure 4 Photomicrographs of calcareous nannofossils from ODP Hole 1146A. The scale bars are 5 μm in length. a-1, a-2, Emiliania huxleyi; b-1, b-2, Pseudoemiliania lacunosa; c-1–c-4, Reticulofenestra asanoi; d-1, d-2, Gephyrocapsa parallela; e-1, e-2, large Gephyrocapsa spp.; f-1, f-2, Gephyrocapsa oceanica; g-1, g-2, Gephyrocapsa caribbeanica; h, Calcidiscus macintyrei, i-1–i-3, Discoaster brouweri; j-1–j-4, Discoaster pentaradiatus; k-1–k-4, Discoaster surculus; l-1–l-4, Discoaster tamalis.

180x267mm (300 x 300 DPI)

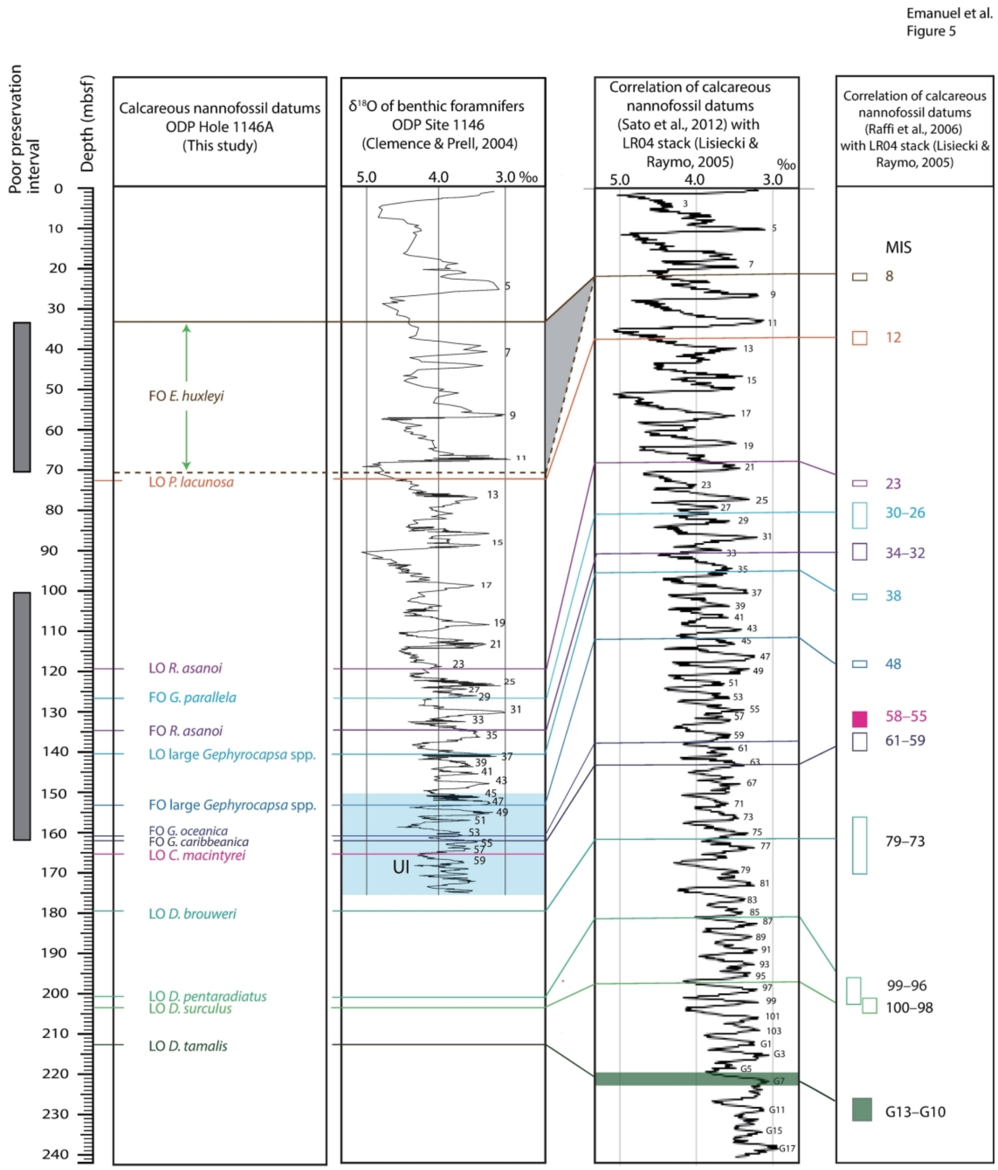

Figure 5 Correlation of the calcareous nannofossil bioevents in the South China Sea (this study) with those of Raffi et al. (2006) and Sato et al. (2012), and compared with the benthic oxygen isotope stratigraphy (BOI) in the South China Sea (Clemence and Prell, 2003) and LR04 stack (Lisiecki and Raymo, 2005). UI = interval in which the BOI stratigraphy does not necessarily show clear cyclicity, preventing reliable correlation with the LR04 stack.

201x244mm (300 x 300 DPI)

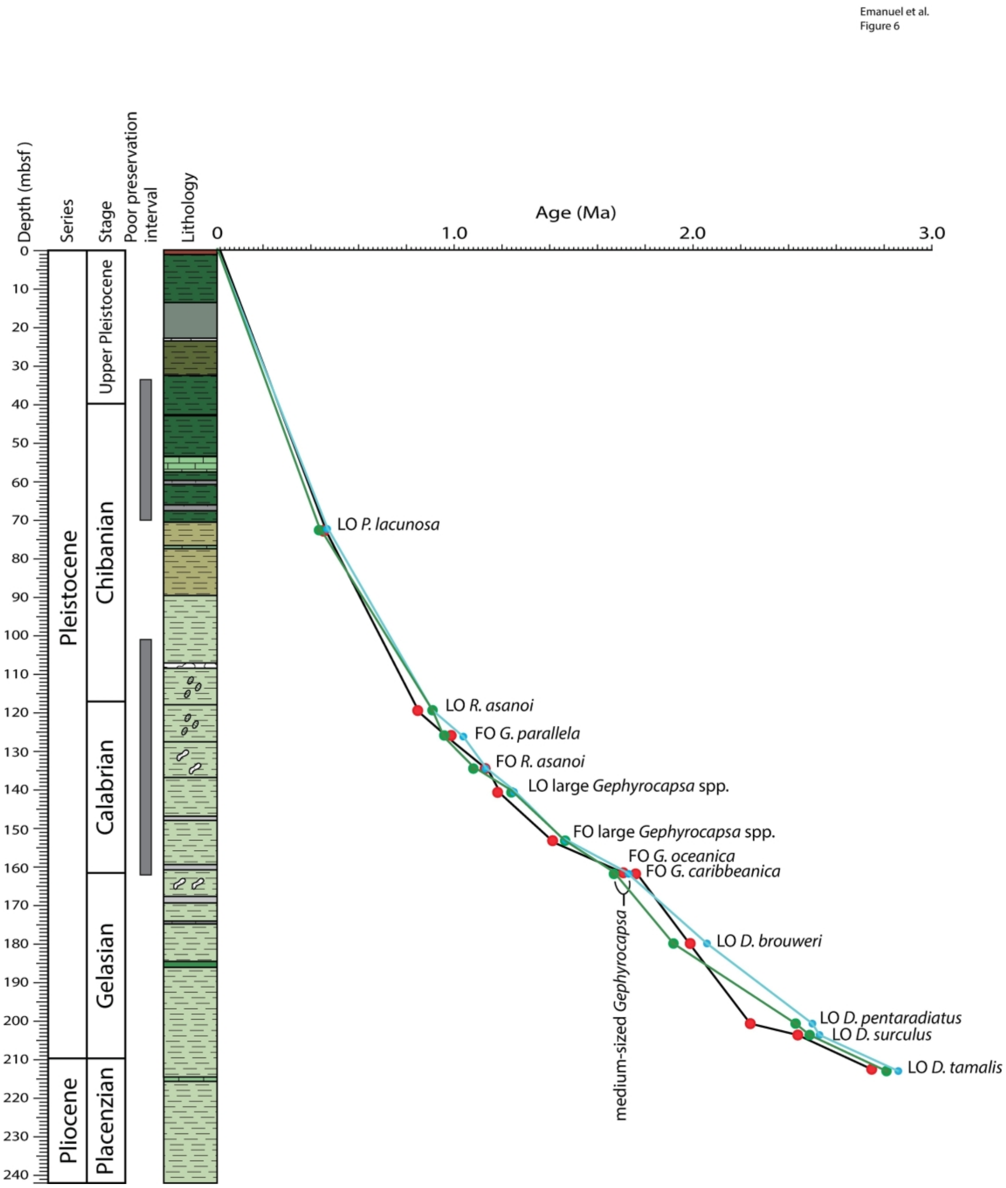

Figure 6 Age–depth plots for the upper Pliocene to Pleistocene succession in the South China Sea, based on calcareous nannofossil datums. Red circles indicate the plots based on the ages of Sato et al. (2012). Green and blue circles indicate the plots based on the ages assigned by Raffi et al. (2006). For the legend see Fig. 2.

193x227mm (300 x 300 DPI)